Monthly Notices
of the
ROYAL ASTRONOMICAL SOCIETY

MNRAS **437,** 132–146 (2014)
Advance Access publication 2013 October 24

doi:10.1093/mnras/stt1863

RATS-*Kepler* – a deep high-cadence survey of the *Kepler* field

Gavin Ramsay,[1]⋆ Adam Brooks,[1,2] Pasi Hakala,[3] Thomas Barclay,[4,5] David Garcia-Alvarez,[6,7,8] Victoria Antoci,[9] Sandra Greiss,[10] Martin Still,[4,5] Danny Steeghs,[10] Boris Gänsicke[10] and Mark Reynolds[11]

[1]*Armagh Observatory, College Hill, Armagh BT61 9DG, UK*
[2]*Mullard Space Science Laboratory, University College London, Holmbury St Mary, Dorking, Surrey RH5 6NT, UK*
[3]*Finnish Centre for Astronomy with ESO, University of Turku, Väisäläntie 20, FI-21500 PIIKKIÖ, Finland*
[4]*NASA Ames Research Center Institute, Moffett Field, CA 94035, USA*
[5]*Bay Area Environmental Research Institute, Inc., 560 Third St. West, Sonoma, CA 95476, USA*
[6]*Instituto de Astrofsica de Canarias, E-38205 La Laguna, Tenerife, Spain*
[7]*Dpto. de Astrofsica, Universidad de La Laguna, E-38206 La Laguna, Tenerife, Spain*
[8]*Grantecan CALP, E-38712 Brea Baja, La Palma, Spain*
[9]*Stellar Astrophysics Centre, Department of Physics and Astronomy, Aarhus University, Ny Munkegade 120, DK-8000 Aarhus C, Denmark*
[10]*Department of Physics, University of Warwick, Coventry CV4 7AL, UK*
[11]*Department of Astronomy, University of Michigan, 500 Church Street, Ann Arbor, MI 48109, USA*

Accepted 2013 October 1. Received 2013 September 27; in original form 2013 April 2

ABSTRACT

We outline the purpose, strategy and first results of a deep, high-cadence, photometric survey of the *Kepler* field using the Isaac Newton Telescope on La Palma and the MDM 1.3 m Telescope on Kitt Peak. Our goal was to identify sources located in the *Kepler* field of view which are variable on a time-scale of a few minutes to 1 h. The astrophysically most-interesting sources would then have been candidates for observation using *Kepler* using 1 min sampling. Our survey covered ∼42 per cent of the *Kepler* field of view, and we have obtained light curves for 7.1×10^5 objects in the range $13 < g < 20$. We have discovered more than 100 variable sources which have passed our two stage identification process. As a service to the wider community, we make our data products and cleaned CCD images available to download. We obtained *Kepler* data of 18 sources which we found to be variable using our survey, and we give an overview of the currently available data here. These sources include a pulsating DA white dwarf, 11 δ Sct stars which have dominant pulsation periods in the range 24 min to 2.35 h, three contact binaries, and a cataclysmic variable (V363 Lyr). One of the δ Sct stars is in a contact binary.

Key words: asteroseismology – surveys – stars: variables: δ Scuti – white dwarf.

1 INTRODUCTION

The prime objective of the *Kepler* mission is to detect Earth-sized planets orbiting solar-type stars in the habitable zone (Koch et al. 2010). It does this by detecting transits of the host star by the orbiting exoplanet. The light curves which *Kepler* obtained extended over many months and have a precision of parts per million. These data allow models of stellar structure to be tested in a way that has not been possible before (e.g. Bedding et al. 2011). Furthermore, it has led to the unexpected discovery of extreme binary systems such as the '*Heartbeat*' stars which are excellent tests of binary and stellar models (Welsh et al. 2011; Thompson et al. 2012).

Asteroseismology provides the means to probe the masses and compositions of stellar interiors, determine stellar internal rotation profiles, the extent of instability strips and therefore test models of stellar structure and evolution (e.g. Chaplin et al. 2011). To study compact objects such as pulsating white dwarfs, relatively high-cadence observations are essential. For the vast majority of observations made using *Kepler*, the effective exposure time is 30 min ['*Long Cadence*' (LC)]. However, for a much more limited number of stars (512), a shorter effective exposure of 1 min is possible ['*Short Cadence*' (SC)].

Before the launch of *Kepler*, an extensive programme to identify bright G/K dwarfs with minimal stellar activity was carried out. Although a small number of photometric variability surveys were carried out pre-launch (e.g. Hartman et al. 2004; Pigulski et al. 2009; Feldmeier et al. 2011), they were either not especially deep, or did

⋆E-mail: gar@arm.ac.uk

Table 1. The dates of observations made using the 2.5 m INT on La Palma and the 1.3 m MDM Telescope on Kitt Peak. We note the number of individual fields which were subject to a 1 h sequence of short exposures in the *g* band (INT) and *V* band (MDM).

Dates	Telescope	No. of fields
2011 Jul 11–17	INT	49
2011 Aug 01–10	INT	58
2012 May 16–22	MDM	26
2012 Aug 03–12	INT	55

not have wide sky coverage or did not have a cadence shorter than a few minutes. To fill this gap, we started a photometric variability survey (RATS-*Kepler*) in the summer of 2011 using the Wide Field Camera (WFC) on the Isaac Newton Telescope (INT). Sources which were considered astrophysically interesting based on their light curve and colour would then have been the subject of bids to obtain *Kepler* SC observations.

2 PHOTOMETRIC OBSERVATIONS

Our strategy is a modified version of that used by us in the RApid Temporal Survey (RATS) which was carried out using the INT between 2003 and 2010 (Ramsay & Hakala 2005; Barclay et al. 2011). In that project, we obtained a series of 30 s exposures of a given field in white light for 2.0–2.5 h. The resulting light curves had a resulting cadence of ∼1 min and for sources brighter than $g = 21$, the standard deviation (σ) of the light curves was <0.024 mag (Barclay et al. 2011). It led to the discovery of a rare double-mode pulsating sdB star (Ramsay et al. 2006; Baran et al. 2011), pulsating white dwarfs and several dozen distant δ Sct or SX Phe stars (Ramsay et al. 2011).

Since the *Kepler* field of view (116 square degrees) is more than twice the area covered by the RATS project, we decided to increase the number of fields observed per night by obtaining a one hour (rather than a two hour) sequence of short exposures per pointing. Since the photometric precision of *Kepler* SC observations reduces from 12.9 per cent at $g = 19$ to 32.4 per cent at $g = 20$ (this compares with 0.85 per cent at $g = 16$)[1], we also reduced the exposure to 20 s and used the *g*-band filter instead of white light (since sources fainter than $g = 20$ would give high-photometric errors in *Kepler* observations).

During the summer of 2011 and 2012, we obtained data using the 2.5 m INT located on the island of La Palma, and the 1.3 m MDM McGraw-Hill Telescope located on Kitt Peak (see Table 1 for details). Our observations cover 42 per cent of the *Kepler* field. In Fig. 1, we show the position of stars observed in our survey in equatorial coordinates.

2.1 Isaac Newton Telescope

The INT WFC has four CCDs and covers 0.29 degrees squared. The dead time was 30 s, giving a cadence of ∼50 s. We are sensitive to flux variations on time-scales as short as a few minutes in sources with a magnitude in the range $13.5 < g < 21$. Tables A1 and A2 show the dates and field centres of each pointing.

[1] http://keplergo.arc.nasa.gov/CalibrationSN.shtml

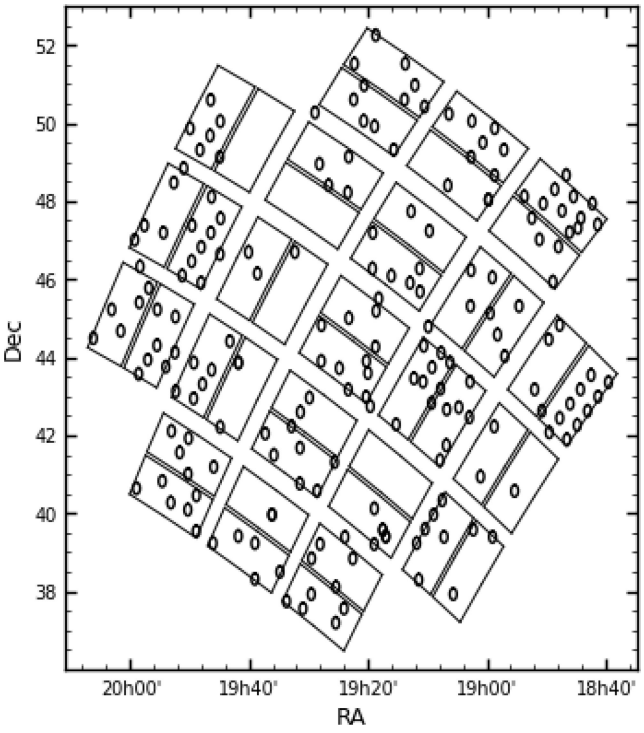

Figure 1. The field centres of our pointings which have been observed to date. Each circle has a diameter of 0.3 square degrees.

2.2 MDM Telescope

The red4k detector was used for two nights and the MDM4k detector for five nights on the MDM Telescope.[2] The field of view in both detectors is 0.12 degrees squared. We used a 30 s exposure in the *V* band for our sequence of observations. For the red4k detector, the readout of 55 s gave a cadence of ∼85 s, while for the MDM4k detector the readout was 40 s, giving a cadence of ∼70 s. For each field, we obtained an image in *BR*, which was then transformed into *gr* magnitudes (Jester et al. 2005) with appropriate normalization to the *Kepler* INT Survey (KIS; Greiss et al. 2012a,b) results. Table A3 shows the dates and field centres of each pointing.

2.3 Image reduction

The data were corrected for the bias level and were flat-fielded using Starlink[3] and FTOOLS[4] software. To embed sky coordinates into the images, we used software made available by ASTROMETRY.NET (Lang et al. 2010). The resulting astrometric positions agreed with the 2MASS source catalogue typically within 0.4 arcsec. We cross-correlated the positions of our sources with that of the KIS (Greiss et al. 2012a,b), which reaches down to a limit of 20 mag in *U*, *g*, *r*, *i* and Hα filters. We also obtained a single *r*-band image of every INT field and a single image of every MDM field in the *BR* filters. We corrected our instrumental magnitudes by scaling them to agree with the KIS values using an offset derived for matched sources.

[2] http://mdm.kpno.noao.edu
[3] http://starlink.jach.hawaii.edu/starlink
[4] http://heasarc.gsfc.nasa.gov/ftools

3 DATA ANALYSIS

We broadly follow the same data reduction and analysis strategy as we used for the RATS project, which is described in Barclay et al. (2011). However, we now outline some features specific to the RATS-*Kepler* project.

3.1 Extracting light curves

The *Kepler* field extends 6°–21° above the Galactic plane. Each of our individual fields are therefore relatively crowded at low latitudes or surprisingly sparse at higher latitudes. For sparse fields, we used SExtractor (Bertin & Arnouts 1996) to extract magnitudes using aperture photometry. Differential magnitudes were determined by comparing the magnitude of each star with the mean brightness of the 3rd–10th most brightest stars in the image (the results were very similar if we chose, say, the 4th–20th most brightest stars). For more crowded fields, we used DIAPL2, an updated version of DIAPL (Wozniak 2000), which extracts photometry by applying the well-established 'Difference Imaging Subtraction' method (Alard & Lupton 1998).

Despite the fact that differential photometry has been performed, we find that the photometry of certain fields suffer from systematic trends in the data – i.e. the light curves derived from the same detector can show similar features. This effect can be seen in many other large-scale surveys, including *Kepler* (Kinemuchi et al. 2012). In our case, the systematic trends will largely result from the fact that for good technical reasons we do not use the autoguider for our INT observations. To ensure that stars remain roughly at the same position on the detector, we apply manual corrections to the pointing.

However, we aimed to remove the effects of systematic trends by applying the SYSREM algorithm (Tamuz, Mazeh & Zucker 2005) to the light curves derived from each CCD individually using a varying number of cycles as described in Tamuz, Mazeh & North (2006) (see also Barclay et al. 2011). For a small number of fields, it was not possible to detrend the data (mainly because of the low number of stars available). Using a faint limit of $g = 20.0$ and a bright limit of $g = 13.5$, we have obtained a total of $7.1\times\ 10^5$ detrended light curves.

3.2 Identifying variable candidates

Identifying *bona fide* variable stars from a large sample of light curves is not a trivial task. Here, we use a two-stage process of identifying variable stars. In the first stage, we use different statistical tests to obtain a sample of candidate variables. In the second stage, we manually perform a quality assessment of each light curve and associated images to remove sources which have been spuriously identified as variable.

Different statistical tests are better suited for identifying different kinds of variability. For instance, the Lomb–Scargle (LS) Periodogram (Lomb 1976; Scargle 1982) is particularly well suited for detecting pulsating variables where the pulsation period is shorter than the duration of the light curve. On the other hand, the Alarm test (Tamuz et al. 2006) and the Analysis of Variance (AoV) test (see Schwarzenberg-Czerny 1989, 1996; Devor 2005 for the implementation used by VARTOOLS) are suitable for identifying eclipsing or contact binaries, whilst the χ^2 test (where the model is the mean magnitude of the light curve) is good for detecting flare stars (see Graham et al. 2013 for a recent review of which tests are best suited for identifying specific kinds of variable star).

The VARTOOLS suite of software (Hartman et al. 2008) allows the parametrization of large numbers of light curves using many different statistical tests in a quick and simple manner. We apply the following tests on each of our light curves: the LS Periodogram, the Alarm test and the AoV test. We also determine the χ^2 value and standard deviation (σ) for each light curve after applying a 5σ clipping to each light curve. A file containing the positions and colours of all sources along with their photometric variability parameters can be downloaded via Armagh Observatory website (star.arm.ac.uk/rats-kepler). Table A4 outlines the full set of parameters which are given in this FITS file.

As an example of how different tests compare, we show in Fig. 2 the results of the σ, LS and AoV tests on a field which contains KIC 3223460 which has a dominant pulsation period of 24.2 min (see Table 2). Plotting the σ of each light curve as a function of g mag shows that KIC 3223460 has a greater σ than the main distribution of sources with similar magnitude. However, there is (naturally) no information on the time-scale of variability. On the other hand, the LS and AoV test clearly identify KIC 3223460 as being strongly variable on a period of 24 min.

The main goal of our survey is to identify compact pulsating stars in the *Kepler* field which would then have been the subject of bids to observe them in SC mode using *Kepler*. As demonstrated in Fig. 2, the LS Periodogram is efficient at identifying these sources in our data. The LS Periodiogram as implemented in VARTOOLS determines the frequency of the highest peak in the power spectrum (which we define as the 'Period' of variability even if the source cannot be verified as strictly periodic) and the false alarm probability (FAP) of this peak being statistically significant. For each light curve, we obtained an LS power spectrum and performed the AoV test in the frequency interval corresponding to the Nyquist frequency (847.1 cycles d^{-1} – which equates to a period of 1.7 min – for the INT data and 600 cycles d^{-1} – which equates to a period of 2.4 min – for the MDM data) and 21.49 cycles d^{-1} – which equates to a period of 67 min – (which is the mean duration of the INT light curves).

For the purposes of selecting an initial sample of candidate variables, we use the LS test. In the absence of red noise and systematic trends, a peak in the power spectrum with log FAP $= -2.5$ is likely to be significantly variable at the 3σ confidence level. However, since the seeing and sky brightness can vary from field to field, and the success of the detrending algorithm can vary from chip to chip, the threshold for identifying variables can be more negative than log FAP $= -2.5$.

We determined the median value of the log FAP statistic for the light curves in each field–chip combination. We then ordered our sources by this median log FAP and made seven subsets containing 10^5 stars each (the remaining 8787 stars which were in field–chip combinations with the highest median log FAP were discarded). For the subset with the least negative mean value for log FAP (Fig. 3), there were 911 sources which has a log FAP < -2.5 (or 0.91 per cent of sources in the subset).

Rather than using a fixed threshold for the log FAP to provide an initial selection of candidate variables, we used the median absolute deviation (MAD) to provide a means of identifying sources which were 'outliers' in the Period–log FAP distribution. The MAD is defined for a batch of parameters $\{x_1, \ldots, x_m\}$ as

$$\mathrm{MAD} = \mathrm{median}_i(|X_i - \mathrm{median}_j(X_j)|). \quad (1)$$

We ordered the data by Period and then into 2-min time bin intervals and derived the MAD for each bin. Candidate variables are then selected so that variable sources obey (log FAP) $< \mathrm{MAD}_{\log \mathrm{FAP}} \times n + \mathrm{Median}_{\log \mathrm{FAP}}$, where n is an integer which defines how far a

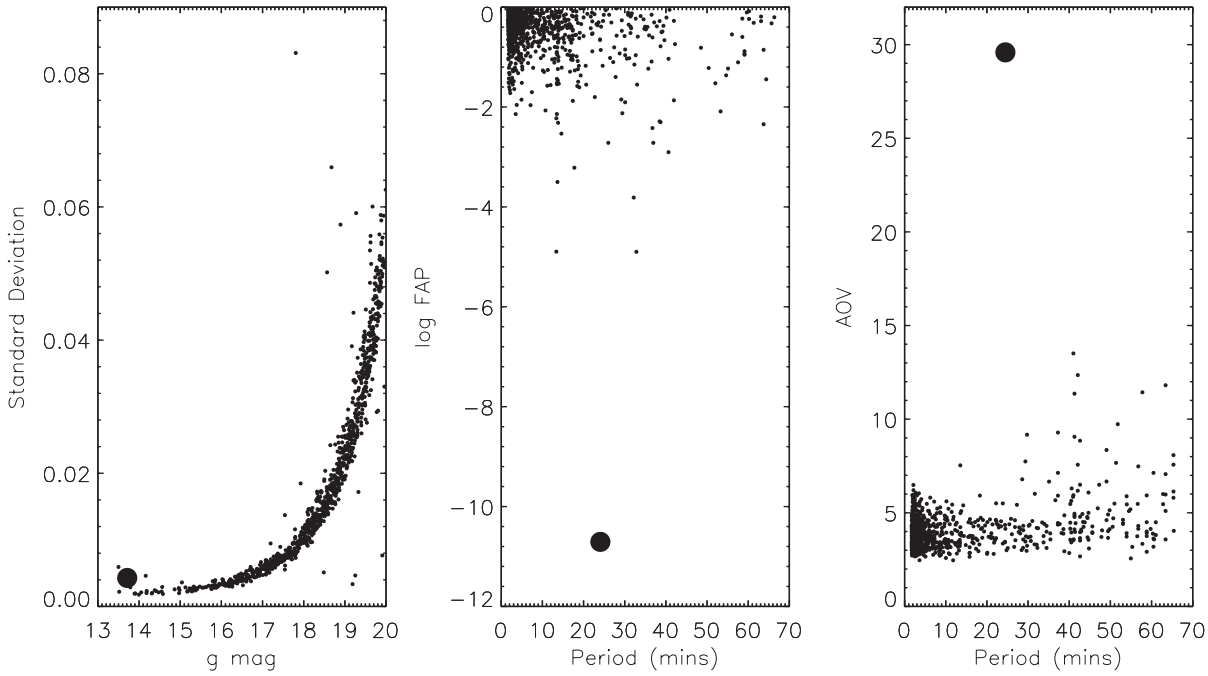

Figure 2. From left to right we plot for all stars in field 73 chip4 (which includes the short period blue variable KIC 3223460) the σ of each light curve as a function of g mag, the log FAP as a function of the period of the highest peak in the LS power spectrum, and the AoV value as a function of the AoV period.

Table 2. The details of those sources whose light curve is shown in Fig. 5. We indicate their KIC ID, their RA and Dec., the g mag, $(U-g)$ and $(g-r)$ colours, which have been taken from the KIS (Greiss et al. 2012a,b). We also show in which quarter *Kepler* SC data were obtained and what the dominant period was in the power spectrum of the *Kepler* light curve. In the 'Spectra' column, we indicate if we obtained a spectrum of the source using the INT or GTC, what the approximate spectral type was and in the last column what the type of variable star the source is. EB: eclipsing binary.

KIC	RA (J2000)	Dec. (J2000)	g	$U-g$	$g-r$	*Kepler* SC data	Period *Kepler*	Spectra	Spectral type	Variable Type
11911480	19 20 24.9	+50 17 22.4	18.13	−0.39	0.06	12,16	290 s			DAV[a]
3223460	19 12 32.2	+38 23 00.1	13.74	−0.27	0.25	14	24.2 min	GTC	Mid–late A	δ Sct
6547396	19 53 18.3	+41 58 26.9	14.84	0.40	0.46	16	26.6 min	INT	Mid–late A	δ Sct
8120184	19 54 11.9	+43 59 20.1	14.27	0.36	0.51	15	42.6 min	INT	Mid–late A	δ Sct
4377815	19 39 08.1	+39 27 35.9	14.83	0.24	0.34	15	45.7 min	INT	Mid–late A	δ Sct
9364179	19 56 24.5	+45 48 24.1	14.38	0.45	0.43	15	46.8 min	INT	Mid–late A	δ Sct
9640005	19 09 46.3	+46 20 04.1	18.40	0.15	0.21	14–16	49.5 min	GTC	Mid A	δ Sct
8840638	19 55 35.1	+45 04 46.0	14.63	0.52	0.54	14–16	49.6 min	GTC	Mid–late A	δ Sct
4636671	19 01 52.2	+39 45 59.3	15.67	0.28	0.26	14–16	50.0 min	GTC	Mid A	δ Sct
12406812	19 23 33.8	+51 17 58.9	17.24	0.18	0.36	14–16	50.4 min	GTC	Mid–late A	δ Sct
5623923	19 32 01.5	+40 51 16.8	16.62	0.23	0.27	14–16	50.5 min	GTC	Mid–late A	EB+δ Scuti
10284901	19 43 46.4	+47 20 32.8	15.73	0.06	0.32	14,16	75.8 min	GTC	Mid–late A	δ Sct
10975348	19 26 46.1	+48 25 30.8	18.89	0.19	0.34	14–16	2.35 h	GTC	Mid A	δ Sct
7431243	19 08 51.6	+43 00 31.5	19.10	−0.94	0.47	16	4.68 h			CV[b]
7667885	19 03 30.2	+43 23 22.7	17.64	1.05	0.95	14–16	7.56 h	GTC	Mid G	W UMa
9786165	19 50 11.0	+46 34 40.8	17.67	0.81	0.76	14,16	7.98 h	GTC	Mid G	W UMa
12553806	19 14 41.0	+51 31 08.9	17.52	0.14	0.41	14–16	11.12 h	GTC	A+F?	W UMa
5474065	19 53 02.5	+40 40 34.6	18.77	1.93	1.43	14	Flare	GTC	M3 V	Flare star[c]

Notes: [a]Greiss et al. (2013), [b]CV(Scaringi et al. 2013), [c]Ramsay et al. (2013).

source is from the local median log FAP. It is selected largely by trial and error – too high a value of n will select only the most strongly variable sources, but too low a value of n will produce large quantities of candidate variables, all of which require manual verification. (To be selected as a candidate variable, a source also has to have log FAP < -2.5). The selection of variables using the MAD statistic was performed on each subset of 10^5 stars separately and then combined according to the n value that was used. We found that for $n = 18$, 227 stars (or 0.032 per cent of the total) were selected as candidate variables ($n = 16 \rightarrow 368$ stars, $n = 14 \rightarrow 642$, $n = 12 \rightarrow 1187$, $n = 10 \rightarrow 1999$). We stress that this selection simply identifies those stars which are most likely to be variable.

Each source is then subject to a manual inspection of the light curve and corresponding images to verify their variable nature.

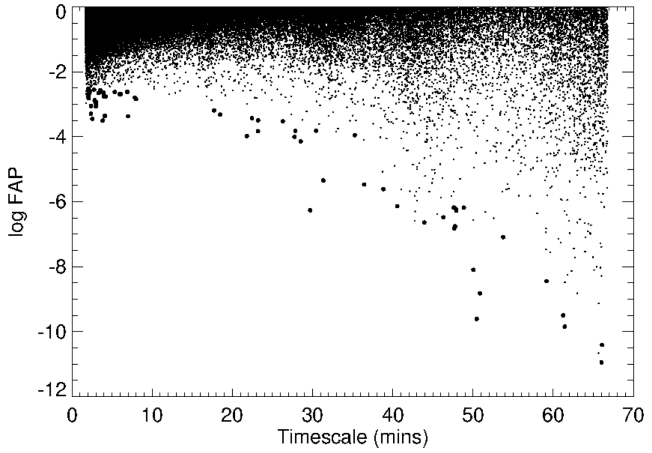

Figure 3. For those 10^5 stars located in field–chip combinations which have the least negative median log FAP, we plot the log of the false alarm probability (FAP) as a function of the period of the most prominent peak in the LS power spectrum. More negative values of log FAP imply a greater chance of intrinsic variability. Those sources which have been identified as variable candidates using the MAD statistic with $n = 14$ are shown as larger filled circles (see Section 3.2 for details).

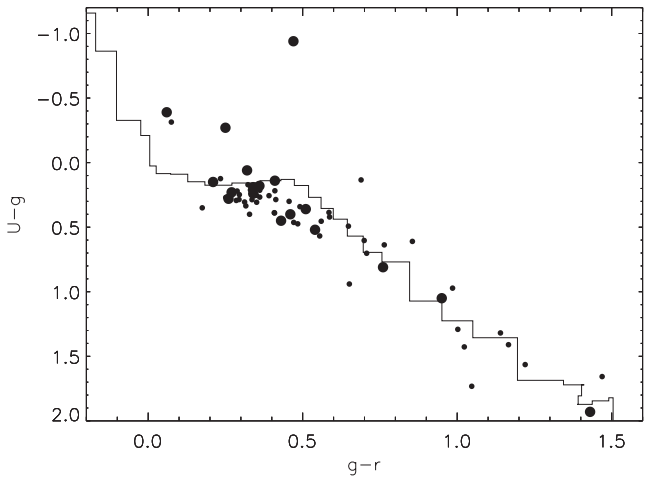

Figure 4. The solid line shows the unreddended main sequence (taken from Groot et al. 2009). Small circles indicate the colours of sources shown in Table A5 while larger circles indicate the colours of those sources which we have obtained using *Kepler* SC data (Table 2).

Where appropriate, additional light curves were obtained using the optimal aperture photometry routine AUTOPHOTOM (Eaton, Draper & Allan 2009). In this process, we assign a Flag value (see Table A4) to characterize their light curve and time-scale of variability. For our $n = 18$ sample, we found that after a second stage verification process we had 65 sources which we classed as highly likely to be variable using the LS statistic at a first screening stage. A summary of these sources is shown in Table A5 and their colours are shown in Fig. 4. By examining samples derived using $n = 14$, we have found more than 100 sources which have passed our two-stage variable identification process. These are indicated in the FITS file which we make available on the Armagh Observatory website.

A high fraction of sources (71 per cent) of the $n = 18$ sample were found unlikely to be *bona fide* variable sources. Many of these spurious variables were caused by residual systematic trends in the light curves – for instance, sources from the same chip showed very similar trends in their light curves. This is almost certainly a result of using manual corrections in the guiding process in the INT observations and for the fact that the light curves only covered a short time (typically 1 h).

We selected 18 sources which would be good targets to observe using *Kepler* in 1-min sampling mode. We successfully bid for *Kepler* Guest Observer Programme and the Directors Discretionary Time Programme. We show the INT light curves of these sources in Fig. 5, and we give their sky coordinates, magnitude and colours in Table 2. We indicate an approximate spectral classification using our INT and Gran Telescopio Canarias (GTC) spectra (Section 4). Of these 18 sources, one is a pulsating DA white dwarf (the details are presented in Greiss et al. 2013), three are contact binaries, one is a cataclysmic variable (CV) and one is a flare star (Ramsay et al. 2013). However, most of these sources appear to be δ Sct stars. We will present an overview of the *Kepler* data of these sources in Section 5.

4 OPTICAL SPECTROSCOPY

As part of our follow up programme, we obtained low–medium resolution optical spectroscopy of over 50 sources which were either identified as being variable on a short time-scale or had unusual colours. (One very blue source in our sample, KIC 10449976, has already been reported as an extreme helium star; Jeffery et al. 2013.) We obtained data using the Intermediate Dispersion Spectrograph (IDS) and the R400 grism on the INT between 2012 June 26 and 28 and also using the Optical System for Imaging and Low Resolution Integrated Spectroscopy (OSIRIS) tunable imager and spectrograph and the R1000R grism on the 10.4 m GTC during 2013 March–June. Both are located at the Observatorio Roque de los Muchachos in La Palma, Canary Islands, Spain. At least two spectra were obtained of each source and the individual exposure time ranged from 180 to 360 s (INT) and 40 to 400 s (GTC). The spectra were reduced using standard procedures with the wavelength calibration being made using a CuNe+CuAr arc taken shortly after the object spectrum was taken. A flux standard was observed so that the (resulting combined) spectra of each source could be flux calibrated in the case of the IDS spectra and to remove the instrumental response in the OSIRIS spectra (the observing programme utilizes poor observing conditions). The spectral resolution of our INT spectra was ∼2 and ∼8 Å for our GTC spectra.

For stars which were of the spectral type A/F, we modelled the spectra using a grid of LTE models calculated using the ATLAS9 code (Kurucz 1992) with convective overshooting switched off. Spectra were calculated with the LINFOR line-formation code (Lemke 1991). Data for atomic and molecular transitions were compiled from the Kurucz line list. The stellar temperatures were estimated from the hydrogen Balmer lines of the stars (Hβ to Hδ) using the FITSB2 routine (Napiwotzki et al. 2004). No gravity-sensitive features are accessible in our low-resolution spectra. McNamara (1997) finds that SX Phe and large amplitude δ Sct stars have a range in log g of 3.0–4.3. In our fits we fixed log $g = 4.0$, although the resulting temperature is only weakly sensitive to this parameter. The metallicity was allowed to vary, although this was not strongly constrained in the fits. The error of the fitted parameters was determined with a bootstrapping method. As an example of the fits, we show in Fig. 6 the fit to the spectrum of KIC 3223460. We show in Table 3 the temperature we derive for the stars for which we have obtained *Kepler* SC data (Section 5). We make all the spectra available through the Armagh Observatory website (http://star.arm.ac.uk/rats-kepler) together with the fitted temperature of each.

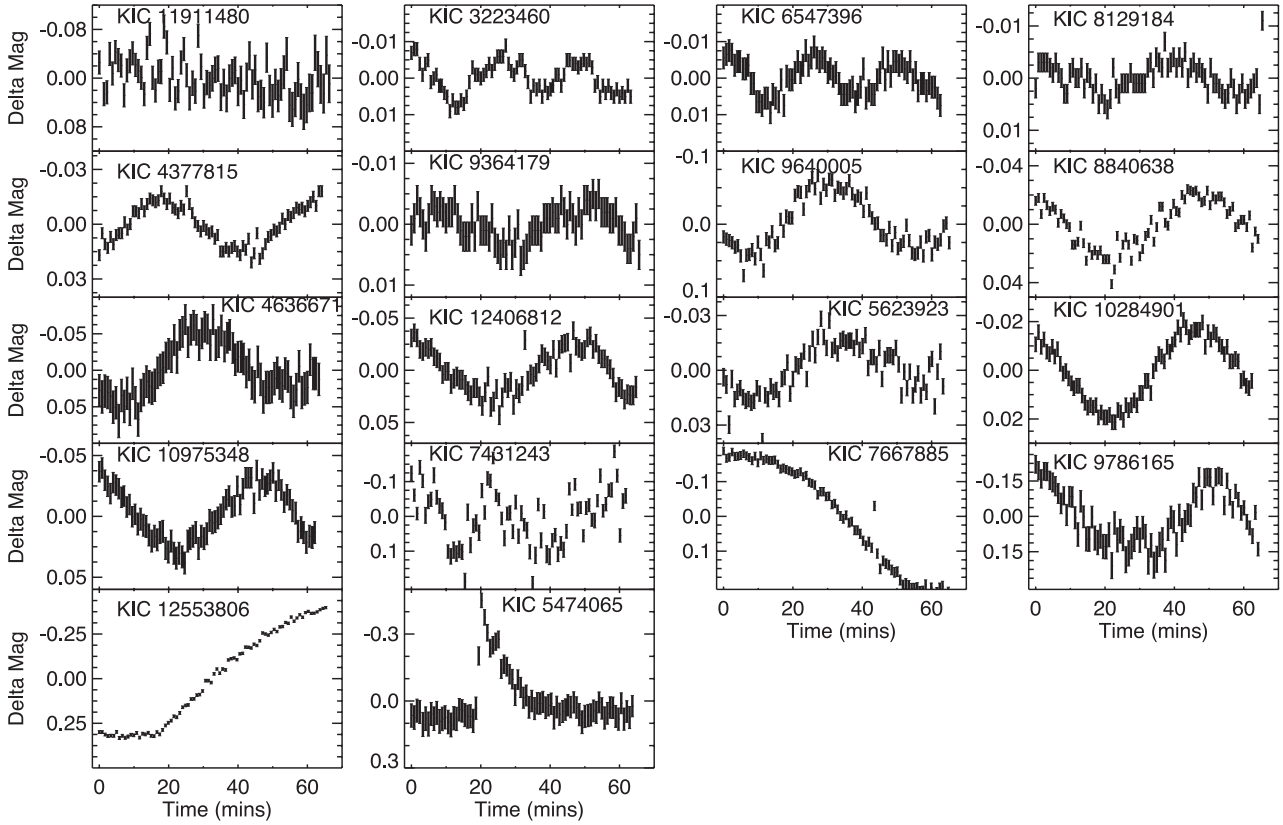

Figure 5. The INT light curve of those sources which have been identified as variable in the *Kepler*-RATS survey and which we have obtained using *Kepler* SC data. The details of these sources are shown in Table 2.

5 *Kepler* OBSERVATIONS

The detector on board *Kepler* is a shutterless photometer using 6 s integrations and a 0.5 s readout. There are two modes of observation: LC, where 270 integrations are summed for an effective 28.4 min exposure, and SC, where 9 integrations are summed for an effective 58.8 s exposure. When an object is observed in SC mode, LC data are also automatically recorded. After the data are corrected for bias, shutterless readout smear and sky background, light curves are extracted using simple aperture photometry (SAP). Data which were contaminated, for instance during intervals of enhanced solar activity, were removed by requiring data to be flagged by the FITS keyword 'SAP_QUALITY' = 0, and the data were corrected for systematic trends (Kinemuchi et al. 2012).

The *Kepler* data on the pulsating DA white dwarf will be presented in full by Greiss et al. (2013) while the *Kepler* data on the flare star KIC 5474065 have been presented by Ramsay et al. (2013). Here, we give a brief overview of the *Kepler* data on the pulsating, contact binaries and CV which we have obtained.

5.1 δ Sct stars

In Table 2, we identify 11 sources which show a dominant period in the range 24.2 min to 2.35 h. Our fits to their low-resolution spectra (Table 3) indicate that they have temperature in the range ∼7600–8300 K. They are therefore consistent with the characteristics of δ Sct and SX Phe stars (see Breger 2000 for a review). We show a short section (1 d) of each of the *Kepler* light curves of these δ Sct type stars in Fig. 7. Using a full month of data, we find that their power spectra are complex and show many frequencies (Fig. 8).

The δ Sct stars with the shortest pulsation periods in our sample are KIC 3223460 (24 min) and KIC 6547396 (26 min). Indeed, they are at the extreme short period end of the δ Sct star distribution (18 min marks the short period end; Uytterhoeven et al. 2011). The discovery of two δ Sct stars with such a short period will therefore provide an opportunity to discover the internal structure of these sources through asteroseismology. Eight of our sample (KIC 8120184, 4377815, 9364179, 9640005, 8840638, 4636671 and 5623923) have a peak in their power spectra which lies in the range 42.6–50.5 min. They have a best-fitting temperature in the range 7660–7950 K (Table 3). The longest period pulsators, KIC 10284901 (75.8 min) and 10975348 (2.35 h) also show high-amplitude variations and appear to be high-amplitude δ scuti stars which occupy a restricted range of the instability strip (McNamara 2000).

Decades of research have shown that the light curves of δ Sct stars are very complex (e.g. Breger 2000; Pamyatnykh 2000). However, this makes them very useful astrophysical laboratories as they show physical phenomena which can be used to test theoretical models. However, in many δ Sct stars, it is difficult to uniquely identify modes in the power spectra of the light curve. An exception is slow rotators, such as 44 Tau (Lenz et al. 2010), where a large variety of pressure and gravity modes were identified. For the majority of these stars, when it comes to modelling their power spectra, a major difficulty is that the mechanism selecting which modes are excited to observable amplitudes is not well understood (Dziembowski & Krolikowska 1990). In other words, some modes are excited while others are not, which makes identifying the specific mode for each peak in the frequency spectra difficult.

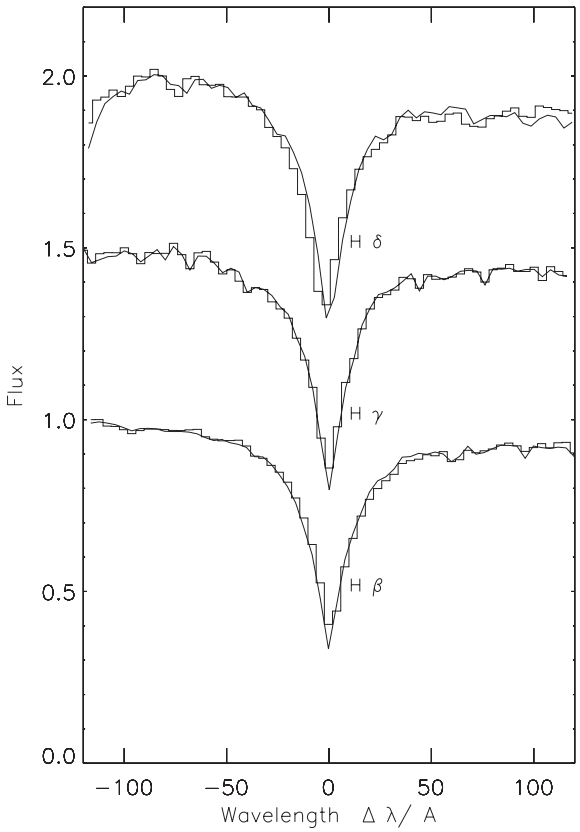

Figure 6. As an example of the spectral fits to our optical spectra, we show the fit to KIC 3223460. For each spectral line, the continuum has been normalized to unity and each spectrum after Hβ has been shifted up by 0.5 flux units.

Table 3. For those sources which we have observed using *Kepler*, we show the temperature we derive from INT and GTC spectra along with the temperature and log g taken from the *Kepler* Input Catalog (Brown et al. 2011). The errors for $T_{\rm GTC}$ and $T_{\rm INT}$ refer to the formal 3σ confidence interval. Including systematic uncertainties, which have not been included, we estimate that the realistic 3σ uncertainties are $\pm$300 K. The uncertainties for $T_{\rm KIC}$ and log $g_{\rm KIC}$ are $\pm$250 K and $\pm$0.25 dex, respectively (cf. Brown et al. 2011; Pinsonneault et al. 2012).

KIC	$T_{\rm GTC}$	$T_{\rm IDS}$	$T_{\rm KIC}$	log $g_{\rm KIC}$
3223460	8180 ± 110		7930	4.1
6547396		8290 ± 110	7480	4.0
8120184		7760 ± 180	7290	3.7
4377815		7880 ± 160	7740	4.0
9364179		7860 ± 180	7000	4.0
9640005	7730 ± 180			
8840638	7860 ± 120		6310	3.8
4636671	7950 ± 120		7640	4.0
12406812	7660 ± 140		7370	4.1
5623923	7970 ± 110		8300	3.9
10284901	7710 ± 180		8420	4.0

The δ Sct stars are stars with masses between 1.5 and 2.5 $M_\odot$ and their pulsations are thought to be driven largely by the opacity mechanism in the He II ionization zone (Baker & Kippenhahn 1962). From *Kepler* and *CoRoT* observations, however, it seems that the opacity mechanism alone cannot excite the entire range of observed modes. This means that either the models are incomplete or that there is an additional mechanism contributing to the driving. Such an alternative explanation would be the presence of stochastically excited modes, like in the Sun. Theoretical models in fact predict that the convective envelopes of δ Sct stars are still deep and effective enough to drive solar-like oscillations. Recently, Antoci et al. (2011) suggested the detection of such a hybrid star, showing κ mechanism and stochastically driven modes. However, longer observations revealed that the interpretation is more complicated than initially anticipated (Antoci et al. 2013). It is therefore of great importance to find pulsating stars with similar temperature and gravity to HD 187547 ($T_{\rm eff}$ = 7500 ± 250 K, log g = 3.9 ± 0.25; Antoci et al. 2011) to test current models. Many of our δ Sct stars have similar temperature to HD 187547 but spectra with higher spectral resolution than the ones we present in Section 4 are required to provide a robust temperature determination. However, even if our δ Sct stars are likely to be too faint to identify their pulsation modes (even the brightest of our sources at g = 13.7 is relatively faint for such an analysis), the frequency range and the stability of excited modes can lead to a better understanding of the pulsation mechanisms, provided the temperature is robustly determined.

5.2 Contact binaries

The *Kepler* data of three of the sources shown in Table 2 and Fig. 5 clearly indicate that they are eclipsing or contact binaries with an orbital period ranging from 0.315–0.463 d. We show the *Kepler* Q14 SC data of these sources in Fig. 9 where we have folded and binned the data on the orbital period.

Prsbrevea et al. (2011) and Slawson et al. (2011) present an analysis of the first and second *Kepler* data release of 4044 eclipsing and contact binaries. Although the shape of the folded light curves of KIC 7667885 and KIC 12553806 are similar to that of semidetached binaries (also known as β Lyr binaries), their relatively short orbital period suggests that they are more likely to be contact binaries (also known as W UMa binaries). The folded light curve of KIC 9786165 also implies that it is a contact binary. Although some caution has to be applied in interpreting the results of our spectral fits since we have applied a single temperature model to sources which are clearly binary systems, the temperatures which we derive (Table 3) indicate that they are contact binaries rather than semidetached binaries which have B-star components (and hence much hotter).

Unlike the three sources outlined here which have been observed using SC mode, none of the sources shown in Prsbrevea et al. (2011) or Slawson et al. (2011) have been observed in SC Mode. Since each of the three binaries have a high inclination, they are excellent data sets to search for third bodies (such as exoplanets) in these systems.

5.3 KIC 5623923: a δ Sct star in a contact binary

We show a 2.5 d section of the light curve of KIC 5623923 in Fig. 10. It is clear that this source is an eclipsing or contact binary system with an orbital period of 1.21 d. However, there are clear pulsations on a period of ∼50 min superimposed on the light curve. The pulsations are not readily apparent during the secondary eclipses indicating that the secondary star (the less luminous of the binary components) is the source of the pulsations.

There are at least two other eclipsing or contact binary stars in the *Kepler* field which have a δ Sct component. KIC 4544587 is a binary system with a 2.18 d orbital period (Hambleton et al. 2013), while KIC 10661783 has an orbital period of 1.23 d (Southworth et al. 2011). Unlike KIC 5623923, where the secondary star is the pulsating component, in both KIC 4544587 and KIC 10661783 the primary is the pulsating star. We note that the spectral fits suggest

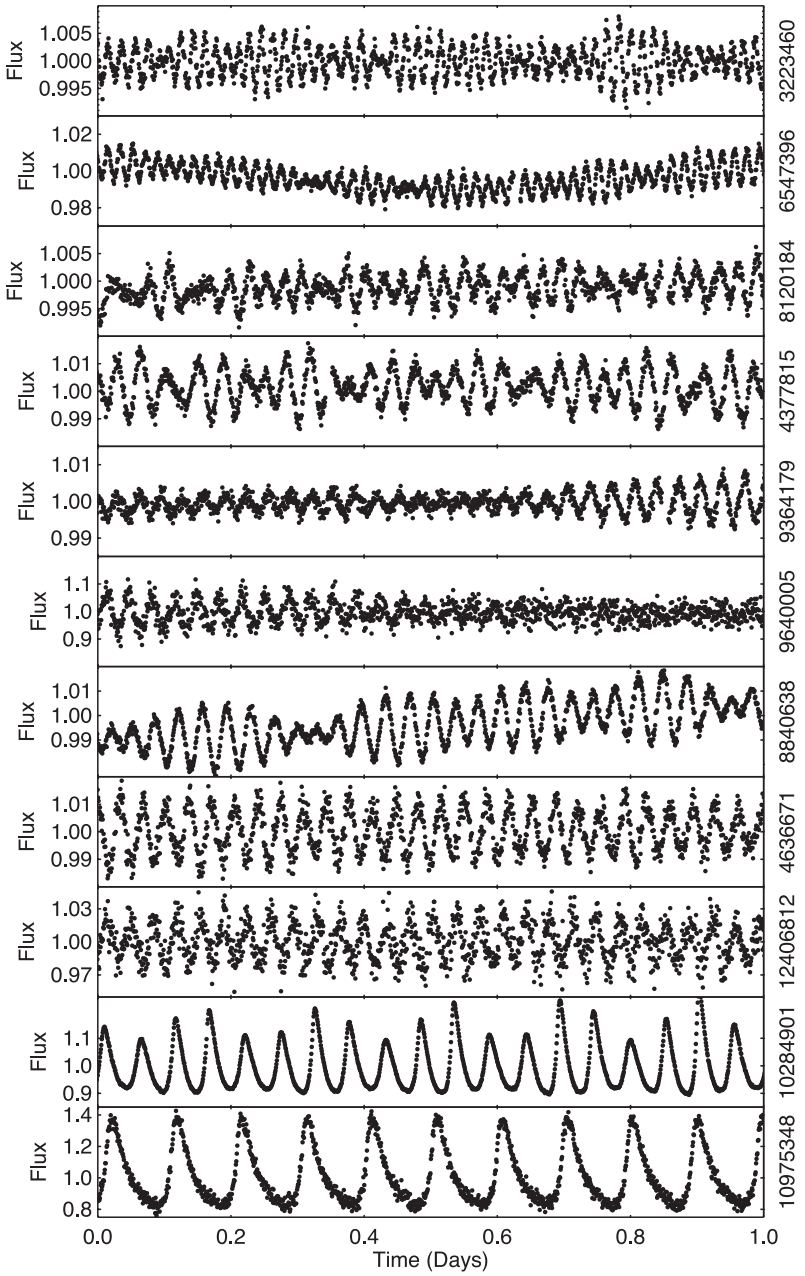

Figure 7. The *Kepler* SC light curves of the 11 sources which appear to be δ Sct type stars. They are ordered so that those showing the shortest dominant period are at the top of the figure. For clarity, we show the light curve covering only one day for each star. The KIC identifier for each star is shown on the right-hand edge of each panel.

a temperature of 8000 K (Table 3), although we have fitted only a single temperature to a system which is clearly a binary.

The power spectrum of KIC 5623923 (Fig. 11) shows many peaks in the 20–30 cycles d^{-1} frequency interval which are due to pressure (p-)mode pulsations in the secondary star. Some of these peaks are separated by 0.83 cycles d^{-1} which is the orbital period. This implies that the amplitude of the δ Sct pulsations are correlated with the orbital period (see Shibahashi & Kurtz 2012 for a discussion on how power spectra can be used to measure radial velocities in binary systems). The power spectrum of KIC 10661783 shows peaks in its power spectrum in a similar frequency range (Southworth et al. 2011), while the p modes seen in KIC 4544587 (Hambleton et al. 2013) are at a higher frequency range (40–50 cycles d^{-1}). We defer a full analysis of these *Kepler* data for a dedicated paper.

5.4 KIC 7431243 (V363 Lyr): a CV

KIC 7431243 was found to be a moderately blue source in the KIS ($g - r = 0.47$; Greiss et al. 2012b) and in our survey it was found to show rapid flux changes superimposed upon an irregular variation (Fig. 5). KIC 7431243 matches the variable star V363 Lyr which was discovered as a CV by Hoffmeister (1967), whilst Kato et al. (2001) found that it shows outbursts of duration 7–8 d every ∼21 d. There are several dozen known CVs in the *Kepler* field (see Howell et al. 2013; Scaringi et al. 2013).

KIC 7431243 was observed using *Kepler* in Q16 for 5.2 d and (not surprisingly) no outbursts were seen (Fig. 12). The power spectrum of the light curve shows peaks corresponding to 4.68 and 4.47 h. If we attribute the longer period to the superhump period

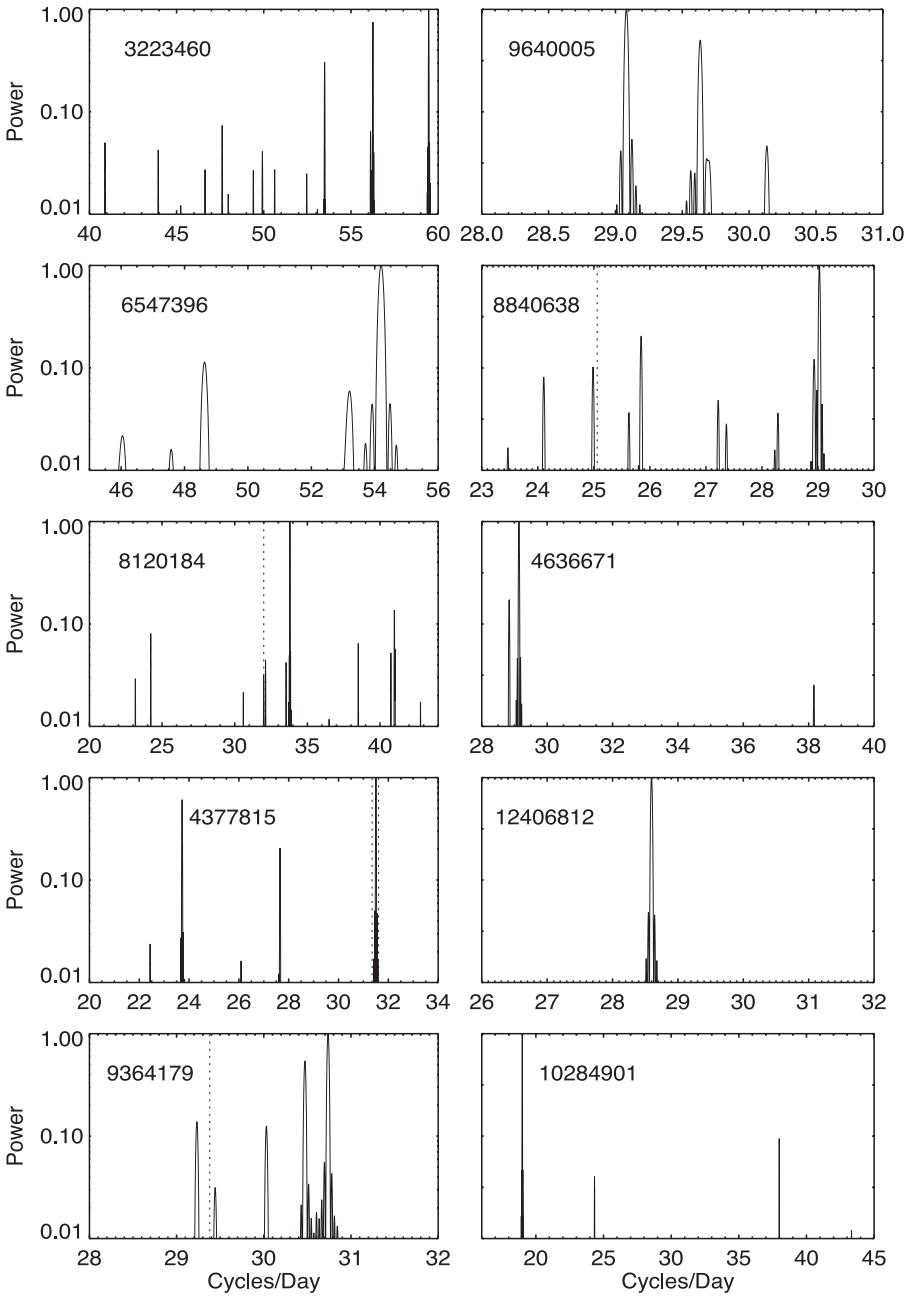

Figure 8. The power spectra of 10 of the sources shown in Fig. 7 (we omit for reasons of space the longest period system shown in Fig. 7). We have normalized the power spectra so that maximum power is unity, plot the power in log space, and we focus on the frequency range of interest in each star. The KIC identifier for each star is shown in each panel. The light curves for each star shown here cover one month of data except for KIC 6547396 where the data were taken in quarter 16 and cover 5.2 d. Dashed vertical lines indicate known artefacts in the power spectra of *Kepler* SC data.

(superhumps are caused by the precession of the accretion disc) and the shorter period to the orbital period, we find the fractional excess, $\epsilon^{+} = (P_{\rm sh} - P_{\rm orb})/P_{\rm orb} = 4.7$ per cent. Using the relationship of Patterson et al. (2005), this would imply a mass ratio, $q = M_2/M_1 \sim 0.21$.

Using the secondary star mass (M_2)–orbital period relationship for CVs ($M_2 = 0.065 P_{\rm h}^{5/4}$; Warner 1995), we find for a CV with $P_{\rm orb} = 4.47$ h, $M_2 = 0.42\,{\rm M}_{\odot}$ ($0.45\,{\rm M}_{\odot}$ for $P_{\rm orb} = 4.68$ h). Superhumps are thought to be restricted to systems where the mass ratio, $q = M_2/M_1 < 0.33$, (see Schreiber 2006 for details). If superhumps are present in KIC 7431243, then this may suggest that the white dwarf in this binary has a mass $M_1 > 1.28\ {\rm M}_{\odot}$ assuming $M_2 = 0.42\,{\rm M}_{\odot}$ ($M_1 > 1.36\ {\rm M}_{\odot}$ for $M_2 = 0.45\,{\rm M}_{\odot}$). Given the potentially high mass of the white dwarf, we urge phase resolved optical spectroscopy this system.

6 CONCLUSIONS

This project set out to identify sources in the *Kepler* field which showed variability on a time-scale of 1 h or less. The most potentially interesting of these variable sources would then have been the subject of bids to obtain *Kepler* data in SC. We have identified more than 100 strongly variable sources, and we have been successful in obtaining *Kepler* SC light curves of 18 of these sources.

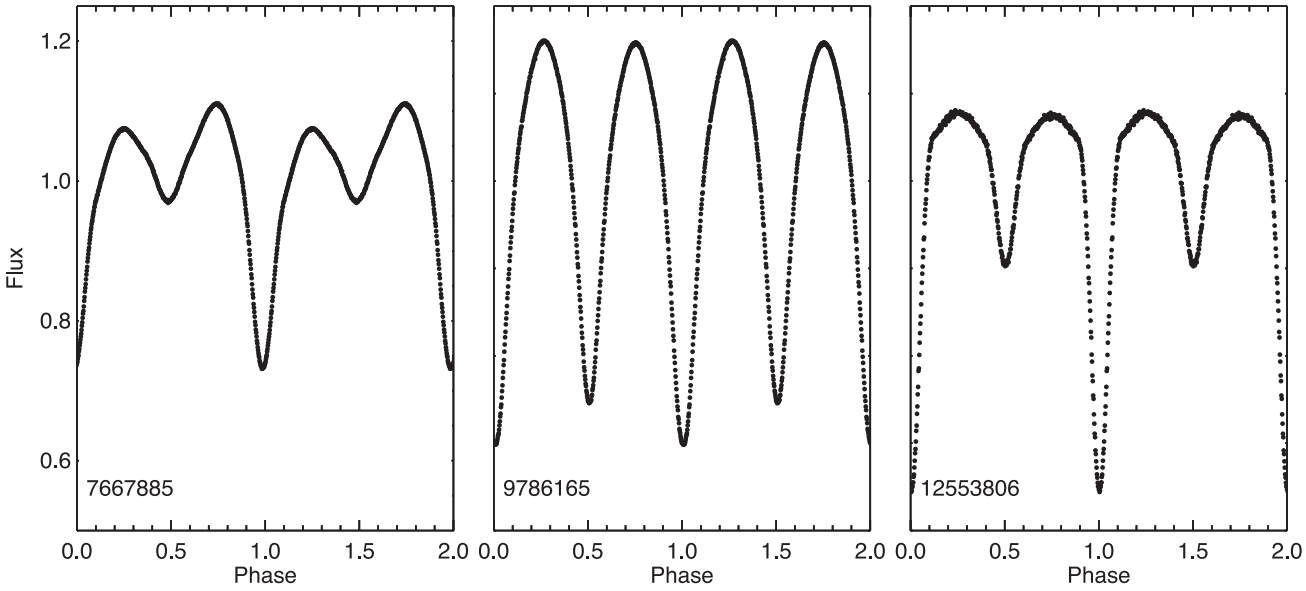

Figure 9. The *Kepler* light curve of the contact binaries KIC 7667885, KIC 9786165 and KIC 12553806. The data have been phased so that the primary eclipse is centred on $\phi = 0.0$ and the y-axis is plotted on the same scale in each panel.

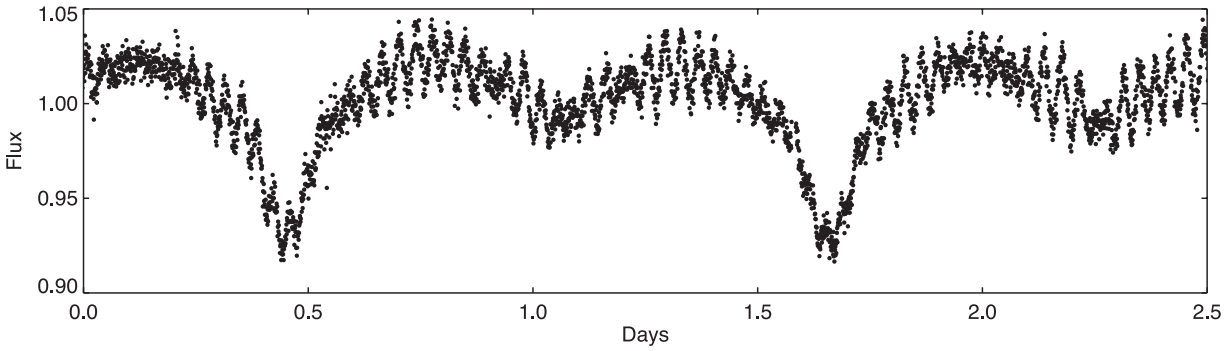

Figure 10. A short section of Q14 *Kepler* data of KIC 5623923. The binary component which is obscured during the secondary eclipse shows clear evidence of pulsations.

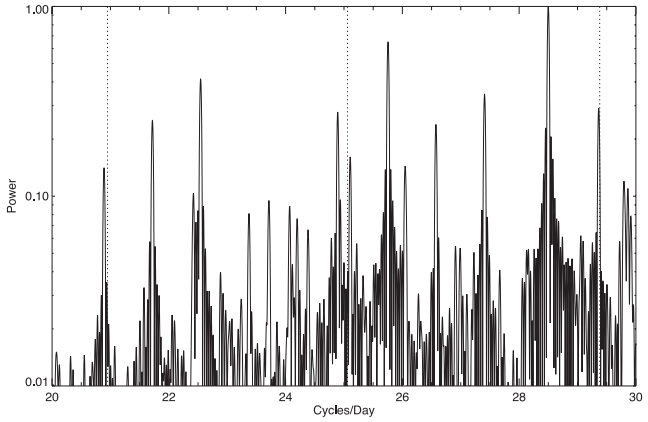

Figure 11. The power spectrum of the Q14 *Kepler* light curve of KIC 5623823. The spacing between some peaks corresponds to the orbital frequency suggesting that the amplitude of the δ Sct pulsations are correlated with the orbital period. Dashed vertical lines indicate known artefacts in the power spectra of *Kepler* SC data.

Many of them are δ Scuti stars which show an astonishing range of variability, the star with the shortest dominant period being 24 min. We also identify one δ Scuti star as being in an eclipsing or contact binary with an orbital period of 1.21 d. As currently only two other such systems are known in the *Kepler* field, this will provide the means to study binary evolution in more detail. We have also obtained *Kepler* SC data of three contact binaries and one previously known CV. The *Kepler* observations of one flare star and one pulsating DA white dwarf are reported elsewhere.

We provide a range of images and data products through the Armagh Observatory website (star.arm.ac.uk/rats-kepler). These include the reduced images so that users can perform photometric measurements using their favoured reduction packages. We also provide the detrended light curves and the photometric variability parameters of each source observed in our survey.

ACKNOWLEDGEMENTS

The INT is operated on the island of La Palma in the Spanish Observatorio del Roque de los Muchachos of the Instituto de Astrofisica de Canarias (IAC) with financial support from the UK Science and Technology Facilities Council. We would like to thank the ING and MDM staff for their support. Observations were also made with

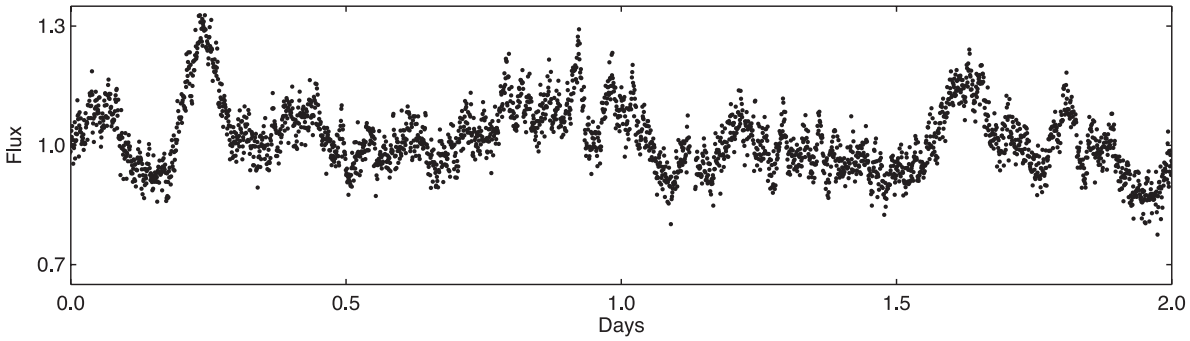

Figure 12. The *Kepler* SC light curve of KIC 7431243 (V363 Lyr) shown over a 2 d time interval.

the GTC which is also sited on La Palma and run by the IAC. Armagh Observatory is supported by the Northern Ireland Government through the Department of Culture, Arts and Lesuire. We thank Wojtek Pych for the use of his difference imaging software DIAPL2. DS acknowledges support of STFC through an Advanced Fellowship. We also thank the referee for helpful comments which helped to significantly improve the paper. Funding for the Aarhus Stellar Astrophysics Centre is provided by The Danish National Research Foundation. The research is supported by the ASTERISK project (ASTERoseismic Investigations with SONG and *Kepler*) and funded by the European Research Council (Grant agreement no.: 267864).

REFERENCES

Alard C., Lupton R. H., 1998, ApJ, 503, 325
Antoci V. et al., 2011, Nature, 477, 570
Antoci V. et al., 2013, MNRAS, 435, 1563
Baker N., Kippenhahn R., 1962, Z. Astrophys., 54, 114
Baran A. S., Gilker J. T., Fox-Machado L., Reed M. D., Kawaler S. D., 2011, MNRAS, 411, 776
Barclay T., Ramsay G., Hakala P., Napiwotzki R., Nelemans G., Potter S., Todd I., 2011, MNRAS, 413, 2696
Bedding T. R. et al., 2011, Nature, 471, 608
Bertin E., Arnouts S., 1996, A&AS, 117, 393
Breger M., 2000, in Breger M., Montgomery M., eds, ASP Conf. Ser. Vol. 210, Delta Scuti and Related Stars. Astron. Soc. Pac., San Francisco, p. 3
Brown T. M., Latham D. W., Everett M. E., Esquerdo G. A., 2011, AJ, 142, 112
Chaplin W. J. et al., 2011, Science, 332, 213
Devor J., 2005, ApJ, 628, 411
Dziembowski W., Krolikowska M., 1990, Acta Astron., 40, 19
Eaton N., Draper P. W., Allan A., 2009, Starlink User Note, 45
Feldmeier J. J. et al., 2011, AJ, 142, 2
Graham M. J., Drake A. J., Djorgovski S. G., Mahabal A. A., Donalek C., Duan V., Maher A., 2013, MNRAS, 434, 3423
Greiss S. et al., 2012a, AJ, 144, 24
Greiss S. et al., 2012b, preprint (arXiv:1212.3613)
Greiss S., Gaensicke B. T., Hemes J. J., Steeghs D. T., Koester D., Ramsay G., Barclay T., 2013, MNRAS, submitted
Groot P. J. et al., 2009, MNRAS, 399, 323
Hambleton K. M. et al., 2013, MNRAS, 434, 925
Hartman J. D., Bakos G., Stanek K. Z., Noyes R. W., 2004, AJ, 128, 1761
Hartman J. D., Gaudi B. S., Holman M. J., McLeod B. A., Stanek K. Z., Barranco J. A., Pinsonneault M. H., Kalirai J. S., 2008, ApJ, 675, 1254
Hoffmeister C., 1967, Astron. Nachr., 289, 205
Howell S. B. et al., 2013, AJ, 145, 109
Jeffery C. S. et al., 2013, MNRAS, 429, 3207
Jester S. et al., 2005, AJ, 130, 873
Kato T., Nogami D., Baba H., Masuda S., 2001, Inf. Bull. Var. Stars, 5118, 1
Kinemuchi K., Barclay T., Fanelli M., Pepper J., Still M., Howell S. B., 2012, PASP, 124, 963
Koch D. G. et al., 2010, ApJ, 713, L79
Kurucz R. L., 1992, Rev. Mex. Astron. Astrofis., 23, 181
Lang D., Hogg D. W., Mierle K., Blanton M., Roweis S., 2010, AJ, 139, 1782
Lemke M., 1991, Internal Report, Department of Astronomy, Univ. Texas at Austin
Lenz P., Pamyatnykh A. A., Zdravkov T., Breger M., 2010, A&A, 509, A90
Lomb N. R., 1976, Ap&SS, 39, 447
McNamara D. H., 1997, PASP, 109, 1221
McNamara D. H., 2000, in Breger M., Montgomery M., eds, ASP Conf. Ser. Vol. 210, Delta Scuti and Related Stars. Astron. Soc. Pac., San Francisco, p. 373
Napiwotzki R. et al., 2004, in Hilditch R. W., Hensberge H., Pavlovski K., eds, ASP Conf. Ser. Vol. 318, Spectroscopically and Spatially Resolving the Components of the Close Binary Stars. Astron. Soc. Pac., San Francisco, p. 402
Pamyatnykh A. A., 2000, in Breger M., Montgomery M., eds, ASP Conf. Ser. Vol. 210, Delta Scuti and Related Stars. Astron. Soc. Pac., San Francisco, p. 215
Patterson J. et al., 2005, PASP, 117, 1204
Pigulski A., Pojmański G., Pilecki B., Szczygieł D. M., 2009, Acta Astron., 59, 33
Pinsonneault M. H., An D., Molenda-Żakowicz J., Chaplin W. J., Metcalfe T. S., Bruntt H., 2012, ApJS, 199, 30
Prsbrevea A. et al., 2011, AJ, 141, 83
Ramsay G., Hakala P., 2005, MNRAS, 360, 314
Ramsay G., Napiwotzki R., Hakala P., Lehto H., 2006, MNRAS, 371, 957
Ramsay G., Napiwotzki R., Barclay T., Hakala P., Potter S., Cropper M., 2011, MNRAS, 417, 400
Ramsay G., Doyle J. G., Hakala P., Garcia-Alvarez D., Brooks A., Barclay T., Still M., 2013, MNRAS, 434, 2451
Scargle J. D., 1982, ApJ, 263, 835
Scaringi S., Groot P. J., Verbeek K., Greiss S., Knigge C., Körding E., 2013, MNRAS, 428, 2207
Schreiber M. R., 2006, A&A, 466, 1025
Schwarzenberg-Czerny A., 1989, MNRAS, 241, 153
Schwarzenberg-Czerny A., 1996, ApJ, 460, L107
Shibahashi H., Kurtz D. W., 2012, MNRAS, 422, 738
Slawson R. W. et al., 2011, AJ, 142, 160
Southworth J. et al., 2011, MNRAS, 414, 2413
Tamuz O., Mazeh T., Zucker S., 2005, MNRAS, 356, 1466
Tamuz O., Mazeh T., North P., 2006, MNRAS, 367, 1521
Thompson S. E. et al., 2012, ApJ, 753, 86
Uytterhoeven K. et al., 2011, A&A, 534, A125
Warner B., 1995, Cataclysmic Variable Stars. Cambridge Univ. Press, Cambridge
Welsh W. F. et al., 2011, ApJS, 197, 4
Wozniak P. R., 2000, Acta Astron., 50, 421

APPENDIX A: TABLES

Table A1. List of fields observed using in the INT in 2011, field ID corresponds to our own internal designations, field centres correspond to a point in CCD 4.

Date (dd-mm-yy)	Field ID	RA Dec. (J2000)	Date (dd-mm-yy)	Field ID	RA Dec. (J2000)
11-07-11	522	19:46:51 +49:43:35	02-08-11	382	19:22:42 +50:39:03
11-07-11	542	19:45:05 +47:36:21	02-08-11	408	19:23:33 +49:11:06
11-07-11	541	19:46:43 +47:14:21	03-08-11	46	19:01:23 +40:59:18
11-07-11	349	19:39:18 +39:16:51	03-08-11	63	19:05:58 +37:58:36
11-07-11	539	19:49:56 +46:30:21	03-08-11	260	19:11:38 +46:19:02
11-07-11	567	19:57:19 +43:59:07	03-08-11	73	19:11:46 +38:20:36
11-07-11	570	19:52:40 +45:05:09	03-08-11	259	19:13:14 +45:57:02
12-07-11	94	18:44:31 +47:36:58	03-08-11	380	19:14:02 +51:34:03
12-07-11	100	18:45:45 +48:09:58	03-08-11	373	19:14:10 +50:39:03
12-07-11	93	18:46:25 +47:14:58	04-08-11	72	19:02:36 +39:37:36
12-07-11	234	18:57:27 +49:21:54	04-08-11	236	19:06:53 +48:26:54
12-07-11	575	19:55:42 +45:16:09	04-08-11	264	19:16:22 +46:08:02
12-07-11	503	19:53:20 +42:09:20	04-08-11	296	19:18:56 +45:13:52
12-07-11	488	19:53:27 +40:19:20	04-08-11	277	19:19:29 +47:14:02
13-07-11	99	18:47:40 +47:47:58	04-08-11	269	19:19:33 +46:19:02
13-07-11	105	18:48:54 +48:20:58	04-08-11	406	19:26:55 +48:27:05
13-07-11	92	18:48:18 +46:52:58	05-08-11	245	19:02:50 +50:05:54
13-07-11	157	19:15:34 +42:19:19	05-08-11	76	19:07:31 +39:26:36
13-07-11	469	19:43:31 +44:27:24	05-08-11	281	19:20:36 +43:01:58
13-07-11	446	19:40:23 +46:44:30	05-08-11	223	19:28:21 +39:15:28
13-07-11	354	19:42:06 +39:27:51	05-08-11	325	19:36:07 +41:32:30
14-07-11	104	18:50:50 +47:58:58	05-08-11	583	20:06:28 +44:32:07
14-07-11	97	18:51:29 +47:03:58	05-08-11	585	20:03:23 +45:16:09
14-07-11	103	18:52:45 +47:36:58	06-08-11	578	20:01:52 +44:43:09
14-07-11	110	18:54:01 +48:09:58	06-08-11	555	19:59:31 +47:03:21
14-07-11	204	19:24:20 +37:36:28	06-08-11	499	19:59:13 +40:41:20
14-07-11	214	19:29:50 +37:58:28	06-08-11	566	19:58:51 +43:37:09
14-07-11	213	19:31:14 +37:36:28	06-08-11	580	19:58:44 +45:27:07
15-07-11	8	18:46:20 +42:51:19	06-08-11	588	19:58:37 +46:22:09
15-07-11	7	18:48:05 +42:29:19	06-08-11	556	19:57:53 +47:25:21
15-07-11	12	18:51:04 +42:40:19	07-08-11	581	19:57:09 +45:49:09
15-07-11	18	18:52:17 +43:13:19	07-08-11	494	19:54:53 +40:52:20
15-07-11	321	19:31:44 +41:43:30	07-08-11	550	19:54:41 +47:14:21
15-07-11	297	19:28:09 +43:56:55	07-08-11	562	19:54:17 +43:48:09
15-07-11	328	19:31:40 +42:38:30	07-08-11	559	19:52:56 +48:31:21
16-07-11	114	18:57:18 +44:04:28	07-08-11	563	19:52:45 +44:10:09
16-07-11	120	18:58:32 +44:37:28	07-08-11	471	19:52:37 +43:10:24
16-07-11	126	18:59:46 +45:10:28	08-08-11	538	19:51:32 +46:08:21
16-07-11	314	19:31:45 +40:48:30	08-08-11	560	19:51:16 +48:53:21
16-07-11	309	19:28:51 +40:37:30	08-08-11	483	19:50:35 +40:08:20
16-07-11	338	19:35:06 +38:32:48	08-08-11	490	19:50:33 +41:03:20
16-07-11	219	19:34:00 +37:47:28	08-08-11	497	19:50:28 +41:58:18
17-07-11	28	18:48:05 +44:52:19	08-08-11	528	19:50:12 +49:54:35
17-07-11	27	18:49:54 +44:30:19	08-08-11	465	19:49:37 +42:59:24
17-07-11	133	18:59:24 +46:05:28	09-08-11	473	19:49:34 +43:54:24
17-07-11	55	18:59:05 +42:16:18	09-08-11	477	19:49:10 +39:35:20
17-07-11	412	19:28:28 +49:00:06	09-08-11	484	19:49:09 +40:30:20
17-07-11	436	19:32:35 +46:44:27	09-08-11	521	19:48:33 +49:21:35
17-07-11	439	19:38:53 +46:11:30	09-08-11	533	19:48:22 +45:57:19
01-08-11	36	18:55:39 +40:37:18	09-08-11	540	19:48:20 +46:52:21
01-08-11	238	19:02:58 +49:10:54	09-08-11	466	19:48:07 +43:21:23
01-08-11	139	19:02:58 +46:16:28	10-08-11	530	19:46:45 +50:38:35
01-08-11	131	19:03:05 +45:21:28	10-08-11	548	19:46:36 +48:09:21
01-08-11	376	19:21:01 +50:06:03	10-08-11	467	19:46:35 +43:43:23
02-08-11	240	18:59:00 +49:54:54	10-08-11	486	19:46:14 +41:14:17
02-08-11	151	19:03:09 +43:25:19	10-08-11	516	19:45:13 +49:10:35
02-08-11	141	19:08:12 +41:24:19	10-08-11	535	19:45:11 +46:41:21
02-08-11	154	19:09:37 +42:52:19	10-08-11	454	19:45:09 +42:15:24
02-08-11	390	19:22:35 +51:34:03			

Table A2. List of fields observed using in the INT in 2012, field ID corresponds to our own internal designations, field centres correspond to a point in CCD 4.

Date (dd-mm-yy)	Field ID	RA Dec. (J2000)	Date (dd-mm-yy)	Field ID	RA Dec. (J2000)
03-08-12	5	18:39:52 +43:24:19	08-08-12	1010	19:20:19 +43:38:30
03-08-12	67	18:59:22 +39:26:36	08-08-12	203	19:25:43 +37:14:28
03-08-12	144	19:03:15 +42:30:19	08-08-12	251	19:06:41 +50:16:54
03-08-12	300	19:23:31 +45:02:56	08-08-12	289	19:19:02 +44:18:58
05-08-12	463	19:42:05 +43:54:24	08-08-12	383	19:20:57 +51:01:03
05-08-12	1001	18:45:00 +47:21:36	09-08-12	1005	19:12:34 +43:30:14
05-08-12	1007	18:59:02 +48:42:37	09-08-12	1006	19:17:19 +39:27:18
05-08-12	155	19:08:06 +43:14:17	10-08-12	1006	19:17:19 +39:27:18
05-08-12	568	19:55:46 +44:21:07	10-08-12	1008	19:11:33 +45:43:44
05-08-12	463	19:42:05 +43:54:24	10-08-12	210	19:25:41 +38:09:28
05-08-12	546	19:49:53 +47:25:22	10-08-12	222	19:29:47 +38:53:28
05-08-12	523	19:45:08 +50:05:35	10-08-12	365	19:15:57 +49:22:03
06-08-12	1	18:46:52 +41:56:18	10-08-12	368	19:10:48 +50:28:03
06-08-12	1002	19:04.62 +42:45:48	10-08-12	374	19:12:25 +51:01:03
06-08-12	168	19:10:56 +44:20:19	11-08-12	1009	19:09:59 +47:17:07
06-08-12	175	19:17:49 +39:37:14	11-08-12	1011	19:18:30 +45:33:11
06-08-12	181	19:19:14 +40:10:15	11-08-12	1012	19:19:12 +49:57:51
06-08-12	305	19:28:07 +44:52:02	11-08-12	292	19:25:07 +43:45:58
06-08-12	342	19:39:19 +38:21:51	11-08-12	359	19:46:21 +39:16:51
07-08-12	1013	19:29:12 +50:19:02	11-08-12	392	19:19:00 +52:18:03
07-08-12	226	19:00:03 +48:04:54	11-08-12	401	19:23:41 +48:16:06
07-08-12	239	19:00:59 +49:32:54	12-08-12	10	18:42:48 +43:35:20
07-08-12	311	19:25:55 +41:21:30	12-08-12	2	18:45:08 +42:18:20
07-08-12	327	19:33:09 +42:16:30	12-08-12	3	18:43:23 +42:40:20
07-08-12	332	19:37:34 +42:05:30	12-08-12	4	18:41:38 +43:02:20
07-08-12	351	19:36:26 +40:00:51	12-08-12	496	19:51:57 +41:36:20
08-08-12	1003	19:06:31 +43:54:48	12-08-12	6	18:49:50 +42:07:20
08-08-12	1004	19:19:55 +42:47:29	12-08-12	9	18:44:35 +43:13:20

Table A3. List of fields observed using the MDM 1.3 m telescope in 2012, field ID corresponds to our own internal designations, field centres correspond to a point approximately in the centre of the chip.

Date (dd-mm-yy)	Field ID	RA Dec. (J2000)	Date (dd-mm-yy)	Field ID	RA Dec. (J2000)
16-05-2012	81	19:12:07 +39:16:50	21-05-2012	174	19:19:15 +39:15:15
16-05-2012	82	19:10:42 +39:38:50	21-05-2012	175	19:17:49 +39:37:15
16-05-2012	83	19:09:16 +40:00:51	21-05-2012	226	19:00:03 +48:04:55
16-05-2012	84	19:07:49 +40:22:55	21-05-2012	351	19:36:26 +40:00:51
17-05-2012	85	18:49:13 +45:58:48	22-05-2012	212	19:22:51 +38:53:28
19-05-2012	135	19:10:10 +44:50:04	22-05-2012	218	19:24:11 +39:26:28
19-05-2012	142	19:07:08 +41:47:26	22-05-2012	273	19:13:03 +47:47:02
19-05-2012	149	19:07:04 +42:42:34	22-05-2012	95	18:42:35 +47:58:58
19-05-2012	89	18:41:41 +47:26:48	23-05-2012	106	18:46:58 +48:42:58
20-05-2012	122	18:54:54 +45:21:28	23-05-2012	286	19:23:37 +43:12:58
20-05-2012	160	19:11:03 +43:25:19	23-05-2012	288	19:20:34 +43:56:58
20-05-2012	161	19:09:32 +43:47:19	23-05-2012	329	19:30:09 +43:00:30
20-05-2012	162	19:08:00 +44:09:19			

Table A4. The full set of parameters which are included in our data products.

Parameter	Notes
KIC_ID	The *Kepler* Input Catalog (Brown et al. 2011) star number;
RA, Dec.	Right Ascension and Declination (J2000);
$g_{\rm mag}$	Taken from the KIS, Greiss et al. (2012a,b);
$g_{\rm err}$	Taken from the KIS, Greiss et al. (2012a,b);
U_g, g_r	$(U-g)$, $(g-r)$ taken from Greiss et al. (2012a,b);
LS_Period	The period of the most prominent peak in the LS periodogram in days and LS_Period_Mins (min);
Log10_LS_Prob	The FAP of the most prominent period in the LS periodogram (in units of log 10);
Alarm	The alarm variability statistic (Tamuz et al. 2006);
AoV_Period	The Period determined from the AoV test in days and AOV_Period_Mins (mins);
AoV	The AoV variability statistic Schwarzenberg-Czerny (1989, 1996);
AOV_SNR	the S/N ratio of the peak measured over the full periodogram;
AOV_NEG_LN_FAP	The negative of the natural logarithm of the formal FAP;
Chi2	The reduced χ^2 value of the light curve tested against the constant mean value (with 5σ clipping);
StdDev	The standard deviation (root mean squared) of the light curve;
Field	Our internal naming convention for the field pointing;
Chip	For the INT/WFC the chip id. There was only one chip for the MDM observations;
FieldChip	The field–chip combination
ID	Our internal naming convention for the source. A six digit number implies the light curve was derived using DIAPL, while for those derived using SExtractor, the numbering system starts from 1;
X,Y	The *X*,*Y* coordinates of the source on the chip;
grats, g_r_rats	The g mag and $(g-r)$ colour at the time of our observations;
Flag	'0' variability on ls_per_min; '1' probable variability on ls_per_min; '2' clear long time-scale high-amplitude variable; '3' not variable on ls_per_min; '4' variable on period other than ls_per_min; '5' possibile variability in general; '6' not likely to be variable; '7' bad light curve; '8' eclipse; '9' possible eclipse; '10' variability likely due to systematic trend; '11' known bad columns on chip; '12' apparent long period could be due to residual systematic trends; '13' image shows close stellar companion;
Tstart, Tstop	The start and end date in MJD of the sequence of g-band observations;
medFAP	The median log FAP for the chip which the source is located.

Table A5. Table showing all of our variable stars selected using '$n = 18$' and which passed our manual verification phase (see Section 3.2) along with a selection of parameters.

KIC ID	RA (J2000)	Dec. (J2000)	$g_{\rm KIS}$ (mag)	$(U-g)_{\rm KIS}$ (mag)	$(g-r)_{\rm KIS}$ (mag)	$g_{\rm rats}$ (mag)	$(g-r)_{\rm rats}$ (mag)	Alarm	AOV Period (min)	AOV	LS_Per (min)	LS_Log_FAP
11911480	19:20:24.91	+50:17:22.4	18.09	−0.39	0.06	18.13	−0.05	0.02	4.89	14.75	4.9	−6.93
8293193	19:17:55.25	+44:13:26.1	18.42	−0.31	0.08	18.41	0.00	1.88	5.17	5.81	5.2	−4.46
	19:29:00.80	+44:56:59.2				13.95		1.43	9.93	9.29	10.1	−5.51
12647528	19:22:50.90	+51:45:31.5	14.31	1.73	1.05	14.35	0.99	2.75	43.4	10.36	10.8	−4.83
10728590	19:23:18.49	+48:02:09.0	19.14		0.97	19.37	1.01	4.25	13.9	8.73	13.8	−4.81
10936077	19:52:53.44	+48:19:35.6	15.85	0.70	0.70	15.90	0.56	2.62	31.8	12.19	16.2	−4.80
7356523	19:19:30.70	+42:58:08.5	19.20	0.94	0.65	19.20	0.65	2.00	18.8	6.91	18.5	−4.44
9899481	19:41:00.84	+46:44:58.3	19.66	0.49	0.64	19.61	0.53	2.99	36.4	10.77	19.3	−5.11
6665002	18:46:27.78	+42:10:34.9	19.50	0.13	0.68	19.45	0.64	3.34	21.0	9.38	21.2	−4.66
8123702	19:57:39.81	+43:55:07.7	13.46	2.04	1.17	13.50	1.11	4.54	64.9	8.78	21.8	−3.98
	18:55:13.43	+43:57:31.6	19.75			19.61	1.08	2.21	22.9	8.10	23.2	−3.83
6109859	19:07:56.19	+41:26:33.1	16.19	0.35	0.17	16.19	0.17	8.22	23.1	39.38	23.4	−11.64
3223460	19:12:32.15	+38:23:00.1	13.71	0.27	0.25	13.74	0.16	7.58	24.4	29.58	24.0	−10.71
	19:53:11.03	+48:39:39.1				14.79	0.63	4.06	44.6	14.76	25.9	−5.42
	19:18:03.08	+39:26:21.8						5.28	26.4	16.88	26.2	−8.03
11360026	19:45:03.62	+49:06:01.0	15.01	0.24	0.29	14.99	0.16	9.25	32.9	18.47	32.5	−9.59
9813390	18:49:08.86	+46:40:04.2	16.86	1.30	1.14	16.98	1.04	10.29	66.2	24.35	34.7	−5.17
10031075	19:54:21.16	+46:57:39.9	15.17	0.63	0.76	15.18	0.64	2.71	38.2	9.62	35.1	−5.57
8118210	19:52:18.66	+43:58:11.8	17.02	0.46	0.47	17.09	0.33	3.98	65.4	12.07	35.4	−6.31
7960631	19:28:05.53	+43:45:45.5	15.31	0.30	0.31	15.32	0.18	7.28	63.5	23.15	35.6	−7.96
9479634	19:48:39.16	+46:03:47.1	14.65	0.39	0.32	14.63	0.20	11.23	36.0	51.00	36.4	−12.4
5772488	19:00:07.98	+41:02:51.8	17.67	0.21	0.33	17.70	0.16	9.54	65.5	22.88	37.3	−8.15
11723564	19:47:11.37	+49:53:13.7	12.81	0.38	0.40	12.74	0.17	7.47	66.4	18.83	38.0	−7.91
10253681	18:46:40.86	+47:18:28.1	17.22	0.60	0.69	17.04	0.63	5.61	37.6	25.38	39.6	−8.51
9786930	19:51:01.55	+46:34:24.6	19.00	1.29	1.00	19.03	0.77	8.33	47.3	18.77	41.1	−6.77
10975348	19:26:46.09	+48:25:30.9	18.88	0.19	0.34	18.72	0.07	13.32	54.0	32.84	41.2	−9.59
9364179	19:56:24.52	+45:48:24.1	14.38	0.44	0.43	14.42	0.36	6.93	43.4	17.11	41.2	−7.51
9294308	19:47:09.39	+45:44:32.1	13.66	0.25	0.34	13.64	0.19	6.09	44.7	17.89	42.9	−8.05

Table A5 – *continued*

KIC ID	RA (J2000)	Dec. (J2000)	g_{KIS} (mag)	$(U-g)_{KIS}$ (mag)	$(g-r)_{KIS}$ (mag)	g_{rats} (mag)	$(g-r)_{rats}$ (mag)	Alarm	AOV Period (min)	AOV	LS_Per (min)	LS_Log_FAP
7698266	19:46:50.79	+43:19:02.3	13.22	0.21	0.41	13.26	0.32	6.54	43.7	18.00	43.6	−7.86
10353926	19:47:53.67	+47:26:56.3	14.89	0.22	0.28	14.90	0.31	9.32	45.0	26.15	44.1	−9.90
7625723	19:47:11.80	+43:16:37.4	14.18	1.42	1.02	14.21	0.95	8.22	48.7	19.43	44.2	−7.70
9417741	19:47:39.58	+45:55:07.6	14.72	0.29	0.28	14.78	0.20	15.78	45.3	75.25	44.4	−13.3
4262791	19:26:48.06	+39:20:35.7	15.74	4.82	0.26	15.71	0.21	13.49	62.9	23.15	44.5	−7.60
12406812	19:23:33.80	+51:17:58.9	17.24	0.17	0.36	17.24	0.21	14.47	46.8	47.66	46.5	−12.06
7548311	19:48:28.48	+43:06:12.3	14.55	0.47	0.48	14.52	0.34	10.56	66.5	32.02	46.7	−9.56
5623923	19:32:01.53	+40:51:16.8	16.61	0.23	0.27	16.57	0.15	10.30	45.3	23.26	47.4	−10.24
6418095	18:44:56.53	+41:50:28.1	13.20	0.12	0.23	13.14	0.23	10.41	47.4	35.16	48.3	−11.61
7770746	19:49:00.55	+43:26:06.4	18.84	1.41	1.16	19.20	1.35	17.02	47.6	72.20	48.5	−13.46
9640005	19:09:46.28	+46:20:04.1	18.39	0.15	0.21	18.39	0.15	18.18	63.9	50.71	48.5	−11.27
9786165	19:50:10.98	+46:34:40.8	17.66	0.81	0.76	18.39	1.12	16.50	47.3	47.53	49.7	−10.19
5474065	19:53:02.53	+40:40:34.6	18.77	1.93	1.43	18.76	1.39	12.75	51.3	105.44	49.9	−6.32
9672731	19:59:30.69	+46:23:06.7	17.47	0.97	0.98	17.95	1.16	8.185	66.2	18.77	51.1	−8.65
8840638	19:55:35.07	+45:04:46.0	14.63	0.52	0.54	14.71	0.42	22.33	49.8	98.99	51.6	−14.54
9720306	19:43:03.19	+46:25:56.0	15.45	0.28	0.33	15.50	0.23	15.80	49.7	30.96	51.9	−10.27
6029053	19:08:02.00	+41:22:12.6	17.51	3.21	1.43	17.51	1.43	13.82	55.1	76.53	52.9	−7.61
8117771	19:51:52.82	+43:55:00.1	13.24	0.26	0.36	13.22	0.25	17.99	54.2	59.45	53.4	−12.18
8387281	19:54:08.13	+44:22:16.5	15.65	1.65	1.47	15.64	1.46	7.73	45.5	49.45	55.6	−6.74
4389023	19:47:47.78	+39:29:41.5	13.63	0.21	0.36	13.64	0.25	18.31	52.3	59.75	56.8	−12.35
5818101	19:54:18.14	+41:04:07.1	17.52	0.25	0.39	17.48	0.28	17.61	65.1	32.50	57.4	−11.32
7839261	19:48:18.90	+43:34:22.1	14.77	0.39	0.40	14.77	0.31	22.00	57.2	92.79	58.0	−13.31
8118471	19:52:35.03	+43:56:42.3	15.72	0.45	0.56	15.75	0.46	12.94	60.8	28.50	59.2	−10.42
5179693	19:18:32.80	+40:22:51.3	17.60	0.17	0.32	17.74	0.29	19.35	65.8	64.82	61.3	−12.62
7768746	19:47:00.08	+43:28:22.2	13.23	0.38	0.58	13.18		18.11	54.1	78.36	61.5	−12.69
3350736	19:34:23.34	+38:24:30.5	15.47	0.30	0.45	15.53	0.33	23.04	64.3	41.69	62.1	−11.50
10284901	19:43:46.41	+47:20:32.8	15.72	0.06	0.31	15.59	0.11	19.40	64.4	161.97	62.1	−13.80
8255272	19:53:55.44	+44:11:49.4	13.24	0.28	0.41	13.18	0.44	17.86	62.1	49.52	63.0	−11.85
9364721	19:57:04.39	+45:48:41.1	19.06	0.60	0.85	19.06	0.71	10.03	64.2	19.32	63.7	−8.99
8908767	19:56:07.19	+45:08:50.8	14.30	0.56	0.55	14.35	0.46	21.59	66.4	118.8	64.0	−14.48
9905251	19:48:41.25	+46:43:33.9	16.11	0.30	0.35	16.13	0.18	17.04	55.9	40.88	64.4	−12.30
9812716	18:47:14.89	+46:36:38.4	13.95	0.28	0.29	13.91	0.14	13.67	52.7	38.82	64.9	−11.91
	19:16:43.60	+39:31:27.8						17.24	62.2	61.85	65.2	−12.21
8254486	19:53:11.74	+44:07:43.2	14.76	0.42	0.58	14.59	0.48	17.17	56.6	47.02	65.2	−12.13
4916020	19:17:58.54	+40:04:54.6	14.57	0.33	0.31	14.53	0.28	13.69	61.9	47.96	65.8	−11.79
4149801	19:18:07.97	+39:15:42.0	19.51	1.56	1.21	19.74	2.04	18.62	54.2	58.62	66.1	−11.72
8561192	19:29:05.17	+44:41:50.8	16.43	0.34	0.49	16.40	0.48	17.05	66.5	62.97	66.5	−10.86

This paper has been typeset from a TEX/LATEX file prepared by the author.